

# Dynamics and stabilization of flexible spacecraft structures with magnetic coil-pair actuators

Bryan Pawlina · Christopher J. Damaren

Received: March 31, 2019 / Accepted: April 29, 2019

**Abstract** The dynamics of flexible spacecraft structures with embedded magnetic actuators are studied. Discretized equations of motion for a constrained plate model and an unconstrained two-plate / rigid bus model are derived for actuators that create in-plane forces via current-carrying coils. Taking inputs to be the magnetic forces generated between pairs of coils, the goal of vibration suppression is shown to result in a bilinear control problem. The selection of a generalized rate output variable is used to obtain a passive map from coil-pair force inputs, yielding  $\mathcal{L}_2$ -stability for strictly passive feedback laws. The implementation of one such feedback corresponds to using collocated sensing at the actuator locations, and given mild assumptions about the actuator location, is a robust stabilizer with respect to unstructured uncertainties. Simulations of the closed-loop system are completed to support findings throughout.

## 1 Introduction

Flexibility is an inherent challenge for large spacecraft with extended structures. Vibration may be brought about from attitude or orbit manoeuvres, thermal stress or deployment of payloads. For vibration control, various actuation schemes have been proposed, including ways of applying transverse forces; such as with thrusters, cables or manipulators [1-3], control moment gyros [4,5]; and piezoelectric actuators [6,7].

Magnetic control schemes have been researched for space applications in various contexts. For instance, positional control of spacecraft using the Lorentz force was studied in [8]. Attitude control using magnetic torques produced using current-carrying loops was studied in [9,10]. Another application of magnetic actuators was found in the use of electromagnetic booms, which have the ability to control attitude and position simultaneously [11]. Two main problems arise in the above schemes. The first is the instantaneous underactuation arising from the cross-product force and torque laws that are inherent to external magnetic field actuation. The second is that the strength of the geomagnetic field decays with the cube of the orbit altitude. The first problem can, in some circumstances, be helped by the fact that the magnetic field in the spacecraft body frame changes as it orbits the Earth, thereby providing average controllability [12].

Arranging current-carrying conductors which produce internal structural forces to affect the vibratory behaviour of space structures was investigated in [13]. The authors conceived of magnetic coils embedded in truss elements which, when activated, served to constrain the deflection of

---

Bryan Pawlina  
Ph.D. Student, University of Toronto Institute for Aerospace Studies  
4925 Dufferin Street, E-mail: bryan.pawlina@mail.utoronto.ca

Christopher J. Damaren  
Professor and Director, University of Toronto Institute for Aerospace Studies  
4925 Dufferin Street, E-mail: damaren@utias.utoronto.ca

the element, thereby altering the bending deflection by means of imposing a moment on a section of the whole structure. This arrangement leads to a linear control system. The advantages of this idea are that the coils interact with each other and therefore don't require a close external magnetic field, and that an electromagnetic system may be less mechanically complex, less massive, and/or higher bandwidth than another option. Our work investigates using forces as feedback laws in discrete actuator locations within continuous structures, for the particular arrangement of "coil-pairs," which are two current loops that are very close together. In contrast with the previous work, the bending deflection of the actual element in which the actuator is located is affected by the stress created by the pair of actuators.

The effect of the in-plane forces on the normal deflection depends on the normal deflection itself. This means that even with linearized dynamics for the attitude and elastic coordinates the controlled dynamics are bilinear. Several problems in which bilinear dynamics emerge are related to elasticity and the resulting state-dependent forcing. For instance, in [14], a thin beam with a tip-mounted electromagnet, controlled by a stationary magnet near the tip produced a bilinear system. In another example, a follower force on the end of a multibody system with flexible joints leads to a bilinear stabilization problem and was examined in [15]. Both of the above studies lead to a quadratic state feedback.

## 2 Magnetic Coil-pairs

The force between two current loops  $a$  and  $b$  is given by [13]:

$$F_{ab} = \frac{I_a I_b \mu_0}{4\pi} \oint_a \oint_b \frac{d\mathbf{l}_b \times (d\mathbf{l}_a \times (\mathbf{r}_a - \mathbf{r}_b))}{|\mathbf{r}_a - \mathbf{r}_b|^3} \quad (1)$$

where  $I_a, I_b$  are the currents in loop  $a$  and loop  $b$  respectively,  $d\mathbf{l}_a, d\mathbf{l}_b$  are the current elements,  $\mathbf{r}_a, \mathbf{r}_b$  are the position of the current elements, and  $\mu_0$  is the vacuum permeability. For two collinear, circular loops, sharing axis  $\hat{z}$  for their axis of symmetry, at a distance  $d$  apart, we can express the quantities in cartesian coordinates:

$$\mathbf{r}_a = [R_a \cos(\theta_a), R_a \sin(\theta_a), -d/2]^T \quad \mathbf{r}_b = [R_b \cos(\theta_b), R_b \sin(\theta_b), d/2]^T \quad (2)$$

$$d\mathbf{l}_a = [-R_a \sin(\theta_a), R_a \cos(\theta_a), 0]^T \quad d\mathbf{l}_b = [-R_b \sin(\theta_b), R_b \cos(\theta_b), 0]^T \quad (3)$$

Which results in the following expression which can be numerically integrated for the force,  $F_{ab}$ :

$$F_{ab} = \frac{I_a I_b \mu_0 d R_a R_b}{4\pi} \int_0^{2\pi} \int_0^{2\pi} \frac{\cos(\theta_a - \theta_b) d\theta_a d\theta_b \hat{z}}{[(R_a \cos(\theta_a) - R_b \cos(\theta_b))^2 + (R_a \sin(\theta_a) - R_b \sin(\theta_b))^2 + d^2]^{3/2}} \quad (4)$$

The key feature is that the force can be compression or tension over a small area proportional to the product of the currents  $I_a$  and  $I_b$ , which may be controlled. Multiple rings can approximate solenoids or similar arrangements.

## 3 Model Dynamics

### 3.1 Structure Modelling

Consider a set of points which comprise a spacecraft  $\mathcal{V}$ , made of elastic parts, labeled  $\mathcal{E}$ , and rigid parts, labeled  $\mathcal{R}$ . The column matrix  $\mathbf{r} = [x, y, z]^T$  specifies points in the spacecraft relative to origin and coordinate frame attached to  $\mathcal{R}$ .

Let the small deflection of an infinitesimal mass element  $dm$  of the spacecraft, expressed in the spacecraft body frame, be given by [4]:

$$\mathbf{w}(\mathbf{r}, t) = \mathbf{w}_0(t) - \mathbf{r}^\times \boldsymbol{\theta}(t) + \begin{cases} \mathbf{u}_e(\mathbf{r}, t), & \mathbf{r} \in \mathcal{E} \\ 0, & \mathbf{r} \in \mathcal{R} \end{cases}, \quad \mathcal{V} = \mathcal{E} \cup \mathcal{R} \quad (5)$$

where  $\mathbf{w}_0$  is the position of the origin,  $\boldsymbol{\theta}$  is the small angular deflection of  $\mathcal{R}$  and  $\mathbf{u}_e$  is the small elastic deflection of  $\mathcal{E}$  with respect to  $\mathcal{R}$ . The skew-symmetric matrix  $\mathbf{r}^\times = \begin{bmatrix} 0 & -z & y \\ z & 0 & -x \\ -y & x & 0 \end{bmatrix}$  implements the cross product operation.

The models under consideration include thin rectangular plates aligned with the body  $z$ -axis, with  $z = 0$  at the midplane. Denoting the out-of-plane deflection by  $w(x, y, t)$ , the displacement field using the Kirchoff-Love assumptions is:

$$\mathbf{u}_e = \left[ -z \frac{\partial w}{\partial x}, -z \frac{\partial w}{\partial y}, w \right] \quad (6)$$

The expression for strain energy due to bending is given by [16]:

$$U_B = \frac{D}{2} \int_{\mathcal{E}_A} \left\{ (\nabla^2 w)^2 + 2(1 - \nu) \left[ \left( \frac{\partial^2 w}{\partial x \partial y} \right)^2 - \frac{\partial^2 w}{\partial x^2} \frac{\partial^2 w}{\partial y^2} \right] \right\} dx dy \quad (7)$$

Where  $\mathcal{E}_A$  denotes the elastic area remaining to be integrated, as we have integrated  $z$  from  $-h/2$  to  $h/2$  and defined the flexural rigidity  $D = \frac{Eh^3}{12(1-\nu^2)}$ , where  $E$  is Young's Modulus and  $\nu$  is Poisson's ratio.

An additional contribution to the strain energy arises from in-plane stress intensities  $N_x$ ,  $N_y$  and  $N_{xy}$  [16]:

$$U_s = \frac{1}{2} \int_{\mathcal{E}_e} \left\{ N_x \left( \frac{\partial w}{\partial x} \right)^2 + N_y \left( \frac{\partial w}{\partial y} \right)^2 + 2N_{xy} \frac{\partial w}{\partial x} \frac{\partial w}{\partial y} \right\} dx dy \quad (8)$$

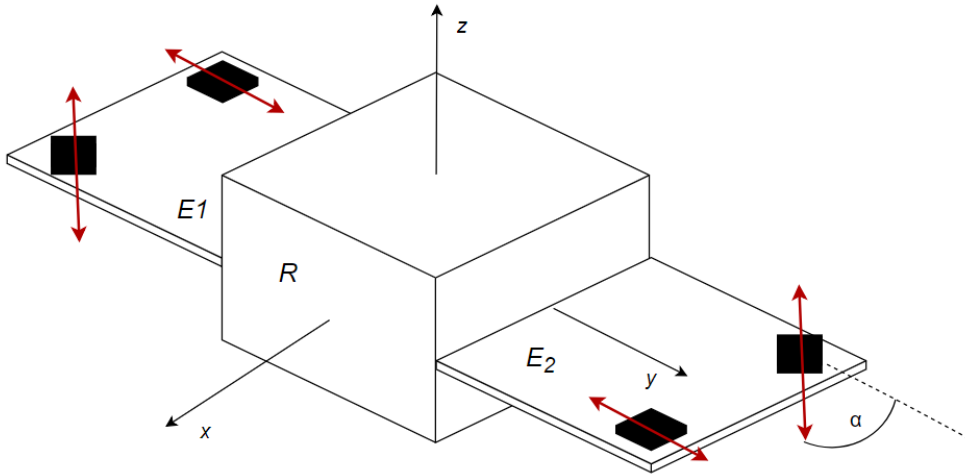


Fig. 1: Unconstrained 2-plate model of rigid (R) spacecraft body with elastic (E1, E2) appendages. Red bi-arrows indicate actuator-induced stress intensities.

Meanwhile, the kinetic energy stemming from the motion of all points in the vehicle is:

$$T = \frac{1}{2} \int_{\mathcal{V}} \rho(\mathbf{r}) \dot{\mathbf{w}}(\mathbf{r}, t)^2 dx dy \quad (9)$$

where  $\rho(\mathbf{r})$  is the mass density. When expanded to include rigid and elastic portions:

$$T = \frac{1}{2} \int_{\mathcal{R}} \rho_{\mathcal{R}} [\dot{\mathbf{w}}_0 - \mathbf{r}^\times \dot{\boldsymbol{\theta}}]^T [\dot{\mathbf{w}}_0 - \mathbf{r}^\times \dot{\boldsymbol{\theta}}] dx dy + \frac{1}{2} \int_{\mathcal{E}} \rho_{\mathcal{E}} [\dot{\mathbf{w}}_0 - \mathbf{r}^\times \dot{\boldsymbol{\theta}} + \dot{\mathbf{u}}_e]^T [\dot{\mathbf{w}}_0 - \mathbf{r}^\times \dot{\boldsymbol{\theta}} + \dot{\mathbf{u}}_e] dx dy \quad (10)$$

To continue, the elastic deflection will be approximated using a finite set of  $N_e$  shape functions  $\psi_i(\mathbf{r})$  and associated time-varying coordinates  $q_{e,i}(t)$ :

$$w(x, y, t) = \sum_{i=1}^{N_e} \psi_i(x, y) q_{e,i}(t) = \boldsymbol{\Psi}(x, y) \mathbf{q}_e(t) \quad (11)$$

The energies in terms of this expansion are written below. Note that differentiation of shape functions is indicated with subscripts while subscripts on  $N$  refer to stress intensity components.

$$U_B = \frac{D}{2} \int_{\mathcal{E}_A} \left[ (\boldsymbol{\Psi}_{xx} + \boldsymbol{\Psi}_{yy}) \mathbf{q}_e \right]^2 + 2(1 - \nu) \left[ (\boldsymbol{\Psi}_{xy} \mathbf{q}_e)^2 + (\boldsymbol{\Psi}_{xx} \mathbf{q}_e)^T (\boldsymbol{\Psi}_{yy} \mathbf{q}_e) \right] dx dy \quad (12)$$

$$U_S = \frac{1}{2} \int_{\mathcal{E}_A} N_x \left[ \boldsymbol{\Psi}_x \mathbf{q}_e \right]^2 + N_y \left[ \boldsymbol{\Psi}_y \mathbf{q}_e \right]^2 + N_{xy} \left[ \boldsymbol{\Psi}_x \mathbf{q}_e \right]^T \left[ \boldsymbol{\Psi}_y \mathbf{q}_e \right] dx dy \quad (13)$$

$$T = \frac{1}{2} \int_{\mathcal{V}} \rho(\mathbf{r}) \left[ \dot{\mathbf{w}}_0 - \mathbf{r}^\times \dot{\boldsymbol{\theta}} + \boldsymbol{\Psi} \dot{\mathbf{q}}_e \right]^T \left[ \dot{\mathbf{w}}_0 - \mathbf{r}^\times \dot{\boldsymbol{\theta}} + \boldsymbol{\Psi} \dot{\mathbf{q}}_e \right] dx dy \quad (14)$$

We apply Hamilton's principle to determine the equations of motion

$$\delta \int_{t_i}^{t_f} [T - (U_B + U_S)] dt = 0 \quad (15)$$

$$\int_{t_i}^{t_f} \delta \dot{\mathbf{q}}^T \mathbf{M} \dot{\mathbf{q}} - \delta \mathbf{q}^T \mathbf{K} \mathbf{q} dt - \int_{t_i}^{t_f} \int_{\mathcal{E}_A} N_x \delta \mathbf{q}_e^T \boldsymbol{\Psi}_x^T \boldsymbol{\Psi}_x \mathbf{q}_e + N_y \delta \mathbf{q}_e^T \boldsymbol{\Psi}_y^T \boldsymbol{\Psi}_y \mathbf{q}_e dx dy = 0 \quad (16)$$

where

$$\mathbf{M} = \begin{bmatrix} m \mathbf{1} & -\mathbf{c}^\times & \mathbf{P} \\ \mathbf{c}^\times & \mathbf{J} & \mathbf{H} \\ \mathbf{P}^T & \mathbf{H}^T & \mathbf{M}_{ee} \end{bmatrix}, \quad \mathbf{K} = \begin{bmatrix} \mathbf{0} & \mathbf{0} & \mathbf{0} \\ \mathbf{0} & \mathbf{0} & \mathbf{0} \\ \mathbf{0} & \mathbf{0} & \mathbf{K}_{ee} \end{bmatrix}, \quad \mathbf{q} = [\mathbf{w}_0^T(t), \boldsymbol{\theta}^T(t), \mathbf{q}_e^T(t)] \quad (17)$$

$m$  is the total mass,  $\mathbf{c}$  is the first moment of mass, and  $\mathbf{J}$  is the moment of inertia of the undeformed spacecraft.

$$\mathbf{P} = \int_{\mathcal{E}} \rho_{\mathcal{E}} [0, 0, \boldsymbol{\Psi}]^T dx dy, \quad \mathbf{H} = \int_{\mathcal{E}} \rho_{\mathcal{E}} \mathbf{r}^\times [0, 0, \boldsymbol{\Psi}]^T dx dy, \quad \mathbf{M}_{ee} = \int_{\mathcal{E}_A} \rho_{\mathcal{E}_A} \boldsymbol{\Psi}^T \boldsymbol{\Psi} dx dy, \quad (18)$$

$$\mathbf{K}_{ee} = \int_{\mathcal{E}_A} D (\boldsymbol{\Psi}_{xx}^T \boldsymbol{\Psi}_{xx} + \boldsymbol{\Psi}_{xx}^T \boldsymbol{\Psi}_{yy} + \boldsymbol{\Psi}_{yy}^T \boldsymbol{\Psi}_{xx} + \boldsymbol{\Psi}_{yy}^T \boldsymbol{\Psi}_{yy} + (1 - \nu) (2 \boldsymbol{\Psi}_{xy}^T \boldsymbol{\Psi}_{xy} - \boldsymbol{\Psi}_{xx}^T \boldsymbol{\Psi}_{yy} - \boldsymbol{\Psi}_{yy}^T \boldsymbol{\Psi}_{xx})) dx dy \quad (19)$$

In the above definition of  $\mathbf{M}$ , bending rotary inertia of the flexible portions has been neglected (terms  $z^2 (\frac{\partial \dot{\mathbf{w}}}{\partial x})^2$ ,  $z^2 (\frac{\partial \dot{\mathbf{w}}}{\partial y})^2$  arising from  $\dot{\mathbf{u}}_e^T \dot{\mathbf{u}}_e$  are considered small).

### 3.2 Effect of Actuators

Only  $N_x$  and  $N_y$  forces have been retained to reflect the effect of the actuators (all in the collinear arrangement). Furthermore, we assume that the inter-coil distance in actuators is much smaller than the distance between actuators and the size of the mode shapes, and so the forces  $N_x$  and  $N_y$  can be modelled as a set of Dirac delta functions at discrete locations:

$$N_x = \sum_{i=1}^m u_i(t) \cos(\alpha_i) \delta_{Dirac}(\mathbf{r} - \mathbf{r}_i), \quad N_y = \sum_{i=1}^m u_i(t) \sin(\alpha_i) \delta_{Dirac}(\mathbf{r} - \mathbf{r}_i) \quad (20)$$

where  $m$  is the number of actuators. Now following an integration by parts on the kinetic term noting the variation is zero at the time interval endpoints we have

$$\int_{t_i}^{t_f} \delta \mathbf{q}^T (-M\ddot{\mathbf{q}} - \mathbf{K}\mathbf{q} - \sum_{i=1}^m u_i(t) \mathbf{\Pi}_i \mathbf{q}) dt = 0 \quad (21)$$

Since the variation  $\delta \mathbf{q}$  is arbitrary within kinematic constraints the equations of motion are

$$M\ddot{\mathbf{q}} + \mathbf{K}\mathbf{q} + \sum_{i=1}^m u_i(t) \mathbf{\Pi}_i \mathbf{q} = 0 \quad (22)$$

where  $\mathbf{\Pi}_i$  are control influence matrices defined as

$$\mathbf{\Pi}_i = \begin{bmatrix} \mathbf{0} & \mathbf{0} & \mathbf{0} \\ \mathbf{0} & \mathbf{0} & \mathbf{0} \\ \mathbf{0} & \mathbf{0} & \mathbf{K}_{c,i} \end{bmatrix}, \quad \mathbf{K}_{c,i} = \left[ \cos(\alpha_i) \mathbf{\Psi}_x^T \mathbf{\Psi}_x + \sin(\alpha_i) \mathbf{\Psi}_y^T \mathbf{\Psi}_y \right] \Big|_{\mathbf{r}=\mathbf{r}_i} \quad (23)$$

and  $\alpha_i$  is the angle the actuator makes in the  $x - y$  plane.

## 4 Stabilization

### 4.1 Constrained Case

Consider the case where a flexible plate is cantilevered on one side to a rigid platform. Such a system with embedded coil-pair actuators would be described by:

$$\mathbf{M}_{ee} \ddot{\mathbf{q}}_e + \mathbf{K}_{ee} \mathbf{q}_e + \sum_{i=1}^m u_i(t) \mathbf{K}_{c,i} \mathbf{q}_e = 0 \quad (24)$$

Matrices  $\mathbf{M}_{ee}$  and  $\mathbf{K}_{ee}$  are symmetric and positive definite. The Lyapunov function  $V = \frac{1}{2} \dot{\mathbf{q}}_e^T \mathbf{M}_{ee} \dot{\mathbf{q}}_e + \frac{1}{2} \mathbf{q}_e^T \mathbf{K}_{ee} \mathbf{q}_e$  is therefore positive definite. Its time derivative is:

$$\dot{V} = \dot{\mathbf{q}}_e^T [\mathbf{M}_{ee} \ddot{\mathbf{q}}_e + \mathbf{K}_{ee} \mathbf{q}_e] = -\dot{\mathbf{q}}_e^T \left[ \sum_{i=1}^m u_i(t) \mathbf{K}_{c,i} \mathbf{q}_e \right] \quad (25)$$

If  $u_i(t) = k_i \mathbf{q}_e^T \mathbf{K}_{c,i} \dot{\mathbf{q}}_e$ , where  $k_i$  is a positive constant then  $\dot{V} = -\sum_{i=1}^m k_i \dot{\mathbf{q}}_e^T \mathbf{K}_{c,i} \mathbf{q}_e \mathbf{q}_e^T \mathbf{K}_{c,i} \dot{\mathbf{q}}_e$ , and the equations become:

$$\mathbf{M}_{ee} \ddot{\mathbf{q}}_e + \sum_{i=1}^m k_i \mathbf{K}_{c,i} \mathbf{q}_e \mathbf{q}_e^T \mathbf{K}_{c,i} \dot{\mathbf{q}}_e + \mathbf{K}_{ee} \mathbf{q}_e = 0 \quad (26)$$

Hence,  $\dot{V}$  is negative semi-definite. If  $\mathbf{q}_e$  is identically zero then the system is in equilibrium, and if  $\dot{\mathbf{q}}_e = 0$ , then  $\ddot{\mathbf{q}}_e$  is also zero, and the only solution to  $\mathbf{K}_{ee} \mathbf{q}_e = 0$  is the origin since  $\mathbf{K}_{ee} > 0$ . It's possible, however, for the expression  $\dot{V} = -(\dot{\mathbf{q}}_e^T \mathbf{K}_{c,i} \mathbf{q}_e)^2$  to be zero for non-trivial trajectories depending on the construction of  $\mathbf{K}_{c,i}$ .

To illustrate the effect of actuator placement on control influence matrices  $\mathbf{K}_{c,i}$ , the Euler-Lagrange equations are written in modal form using eigenvectors  $\mathbf{q}_{e,\beta}$  from the unforced problem:

$$-\omega_\beta^2 \mathbf{M}_{ee} \mathbf{q}_{e,\beta} + \mathbf{K}_{ee} \mathbf{q}_{e,\beta} = 0 \quad (27)$$

which satisfy the orthogonality relations

$$\mathbf{q}_{e,\beta}^T \mathbf{M}_{ee} \mathbf{q}_{e,\gamma} = \delta_{\beta\gamma}, \quad \mathbf{q}_{e,\beta}^T \mathbf{K}_{ee} \mathbf{q}_{e,\gamma} = \omega_\beta^2 \delta_{\beta\gamma} \quad (28)$$

Inserting the modal expansion

$$\mathbf{q}_e(t) = \sum_{\beta=1}^{N_e} \mathbf{q}_{e,\beta} \eta_\beta(t) \quad (29)$$

and left-multiplying by each  $\mathbf{q}_{e,\beta}^T$  we get the modal equations

$$\ddot{\eta}_\beta + \omega_\beta^2 \eta_\beta = - \sum_{i=1}^m \sum_{j=1}^{N_e} u_i(t) \mathbf{q}_{e,\beta}^T \mathbf{K}_{c,i} \mathbf{q}_{e,j} \eta_j \quad (30)$$

Identifying

$$\mathbf{q}_{e,\beta}^T \mathbf{K}_{c,i} \mathbf{q}_{e,j} = \cos(\alpha_i) \mathbf{q}_{e,\beta}^T \Psi_x^T(\mathbf{r}_i) \Psi_x(\mathbf{r}_i) \mathbf{q}_{e,j} + \sin(\alpha_i) \mathbf{q}_{e,\beta}^T \Psi_y^T(\mathbf{r}_i) \Psi_y(\mathbf{r}_i) \mathbf{q}_{e,j} \quad (31)$$

and defining

$$\varphi_{x,\beta}^i = \Psi_x(\mathbf{r}_i) \mathbf{q}_{e,\beta}, \quad \varphi_{y,\beta}^i = \Psi_y(\mathbf{r}_i) \mathbf{q}_{e,\beta} \quad (32)$$

as the natural mode shape derivatives in the x and y directions evaluated at  $\mathbf{r}_i$ , the equations of motion are now:

$$\ddot{\eta}_\beta + \omega_\beta^2 \eta_\beta = -u(t) \left( \cos(\alpha_i) (\varphi_{x,\beta}^i \varphi_{x,1}^i \eta_1 + \varphi_{x,\beta}^i \varphi_{x,2}^i \eta_2 + \cdots + \varphi_{x,\beta}^i \varphi_{x,N_e}^i \eta_{N_e}) + \cdots \quad (33)$$

$$+ \sin(\alpha_i) (\varphi_{y,\beta}^i \varphi_{y,1}^i \eta_1 + \varphi_{y,\beta}^i \varphi_{y,2}^i \eta_2 + \cdots + \varphi_{y,\beta}^i \varphi_{y,N_e}^i \eta_{N_e}) \right) \quad \beta = 1, 2, \dots, N_e \quad (34)$$

We can see from the above that in order for  $\eta_\beta$  to be stabilizable, one of  $\cos(\alpha) \varphi_{x,\beta}$ ,  $\sin(\alpha) \varphi_{y,\beta}$  has to be non-zero. The interpretation is that the actuator must not be placed at a zero-crossing of both spatial derivatives of a mode shape. In Fig. 2, derivative nodal lines are shown for an example mode and the areas where an actuator would be ineffective in controlling that mode identified.

#### 4.2 Unconstrained Case

In the unconstrained case, we can expand the displacement out using

$$\mathbf{q}(t) = \mathbf{Q}_r \boldsymbol{\eta}_r(t) + \sum_{\beta=1}^{N_e} \mathbf{q}_\beta \eta_\beta(t) \quad (35)$$

where  $\boldsymbol{\eta}_r$  are the rigid modes, such that  $\mathbf{K} \mathbf{Q}_r = \mathbf{0}$ . A particular choice is  $\mathbf{Q}_r = \begin{bmatrix} \mathbf{1}_{6 \times 6} \\ \mathbf{0}_{N_e \times 6} \end{bmatrix}$  in which case  $\boldsymbol{\eta}_r = [\mathbf{w}_0(t), \boldsymbol{\theta}(t)]^T$ . The modal system equations are:

$$\begin{bmatrix} m\mathbf{1} & -\mathbf{c}^\times \\ \mathbf{c}^\times & \mathbf{J} \end{bmatrix} \ddot{\boldsymbol{\eta}}_r = \mathbf{0} \quad (36)$$

$$\ddot{\eta}_\beta + \omega_\beta^2 \eta_\beta = - \sum_{i=1}^m \sum_{j=1}^{N_e} u_i(t) \mathbf{q}_{e,\beta}^T \mathbf{K}_{c,i} \mathbf{q}_{e,j} \eta_j \quad \beta = 1, 2, \dots, N_e \quad (37)$$

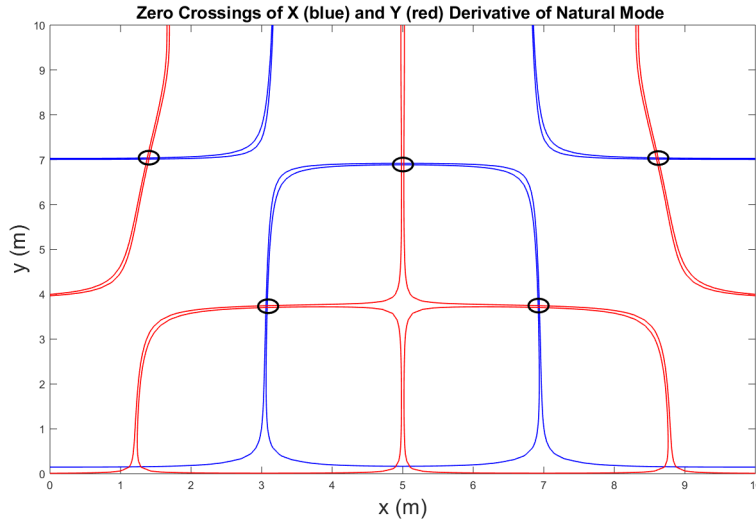


Fig. 2: x-derivative and y-derivative mode shape zero-crossings for mode with  $\omega = 2.986$  rad/s. Black circles represent interior points of zero control authority.  $[Lx, Ly, \nu, D, \rho] = [10\text{m}, 10\text{m}, 0.3, 10\text{Pa m}^3, 1\text{kg/m}^2]$ .

Using a similar Lyapunov function  $V = \frac{1}{2}\dot{\mathbf{q}}^T \mathbf{M}\dot{\mathbf{q}} + \frac{1}{2}\mathbf{q}^T \mathbf{K}\mathbf{q}$ , which is now only semidefinite on account of  $\mathbf{K}$ , leads to  $\dot{V} = -\dot{\mathbf{q}}^T [\sum_{i=1}^m u_i(t) \mathbf{\Pi}_i \mathbf{q}]$ . We can choose, similar to in (26),  $u_i(t) = k_i \dot{\mathbf{q}}^T \mathbf{\Pi}_i \mathbf{q}$  to obtain  $\dot{V} = -\sum_{i=1}^m k_i \dot{\mathbf{q}}^T \mathbf{\Pi}_i \mathbf{q} \mathbf{q}^T \mathbf{\Pi}_i \dot{\mathbf{q}}$ , and the equations of motion will be:

$$\mathbf{M}\ddot{\mathbf{q}} + \sum_{i=1}^m k_i \mathbf{\Pi}_i \mathbf{q} \mathbf{q}^T \mathbf{\Pi}_i \dot{\mathbf{q}} + \mathbf{K}\mathbf{q} = 0 \quad (38)$$

The set of trajectories the system will approach now includes linear solutions in the space of rigid body modes, as the coil-pair actuators act only on the vibration modes. Note that in this case the eigenmodes are now based on the eigenvalue problem:

$$-\omega_\beta^2 \mathbf{M}\mathbf{q}_\beta + \mathbf{K}\mathbf{q}_\beta = 0 \quad (39)$$

and the limitations on actuator placement are based on the unconstrained mode derivative nodal lines, i.e.; different than in the constrained case.

### 4.3 Robustness and Implementation

There are several advantages to analyzing these systems from the perspective of passivity. First, it may facilitate controller design beyond the Lyapunov method above. Secondly, it is known we can represent unmodelled vibration modes as passive mechanical systems, and so if we design a strictly passive feedback law for the controlled dynamics, it will not cause unbounded growth in the uncontrolled signals.

Shortly we will use the partial differential equation (PDE) [16]:

$$D\nabla^2 \nabla^2 w + \rho \ddot{w} = \frac{\partial}{\partial x} \left( N_x \frac{\partial w}{\partial x} \right) + \frac{\partial}{\partial y} \left( N_y \frac{\partial w}{\partial y} \right) \quad (40)$$

Consider the positive definite storage function:

$$V = \frac{1}{2} \int_{\mathcal{E}_d} [D(\nabla^2 w)^2 + \rho \dot{w}^2] dA \quad (41)$$

$$\dot{V} = \frac{1}{2} \int_{\mathcal{E}_d} \frac{\partial}{\partial t} (D(\nabla^2 w)^2 + \rho \dot{w}^2) dA = \int_{\mathcal{E}_d} [D\nabla^2 w \nabla^2 \dot{w} + \rho \dot{w} \ddot{w}] dA \quad (42)$$

$$\dot{V} = \int_{\mathcal{E}_A} [D\nabla^2(\nabla^2 w)\dot{w} + \rho\dot{w}\dot{w}] dA + \oint_{\partial\mathcal{E}_A} \nabla^2 w \frac{\partial\dot{w}}{\partial n} ds - \frac{\partial\nabla w}{\partial n} \dot{w} ds \quad (43)$$

where  $n = (n_1, n_2)$  is the outward unit normal of the plate boundary and  $s = (-n_2, n_1)$  is the unit vector tangent to the boundary. The boundary integral is 0 since on the cantilever side(s),  $\frac{\partial\dot{w}}{\partial n} = 0$  and  $\dot{w} = 0$ , while on the free sides,  $\nabla^2 w = 0$  and  $\frac{\partial\nabla^2 w}{\partial n} = 0$  are statements of zero boundary moment and shear force, respectively. Therefore, substituting the PDE, we have:

$$\dot{V} = \int_{\mathcal{E}_A} \dot{w} \frac{\partial}{\partial x} \left( N_x \frac{\partial w}{\partial x} \right) + \dot{w} \frac{\partial}{\partial y} \left( N_y \frac{\partial w}{\partial y} \right) dA \quad (44)$$

Integrating by parts, noting that stress intensities  $N_x, N_y$  are zero at boundaries and using the sifting property of the Dirac delta function, we get:

$$\dot{V} = - \sum_i^m \left( \cos(\alpha_i) \frac{\partial\dot{w}}{\partial x} \frac{\partial w}{\partial x} + \sin(\alpha_i) \frac{\partial\dot{w}}{\partial y} \frac{\partial w}{\partial y} \right) \Big|_{\mathbf{r}_i} u_i \quad (45)$$

Taking  $\mathbf{y} = \text{col}_i \left\{ - \left( \cos(\alpha_i) \frac{\partial\dot{w}}{\partial x} \frac{\partial w}{\partial x} + \sin(\alpha_i) \frac{\partial\dot{w}}{\partial y} \frac{\partial w}{\partial y} \right) \Big|_{\mathbf{r}_i} \right\}$ , the condition for passivity,  $\dot{V} \leq \mathbf{y}^T \mathbf{u}$ , is satisfied with strict equality. This is the most conservative case as the inequality continues to hold in systems with structural damping.

Strictly passive systems satisfy  $\int_0^T \mathbf{u}^T \mathbf{y} dt \geq \epsilon \int_0^T \mathbf{u}^T \mathbf{u} dt$ ,  $\epsilon > 0$ ,  $\forall T > 0$ . If  $\mathcal{H}_1$  in  $\mathbf{y} = \mathcal{H}_1 \mathbf{u}$  is passive, and  $\mathcal{H}_2$  in  $\mathbf{u} = \mathcal{H}_2 \mathbf{y}$  is strictly passive, then for the feedback interconnection defined by  $\mathbf{y} = \mathcal{H}_1 \mathbf{e} = \mathcal{H}_1(\mathbf{d} - \mathbf{u}) = \mathcal{H}_1(\mathbf{d} - \mathcal{H}_2 \mathbf{y})$ ,  $\mathbf{d} \in \mathcal{L}_2 \implies \mathbf{y} \in \mathcal{L}_2$ , where  $\mathcal{L}_2 = \{\mathbf{u}(t) : \sqrt{\int_0^\infty \mathbf{u}^T \mathbf{u} dt} < \infty\}$ . Stabilization is achieved for any strictly passive feedback in the presence of finite energy disturbances  $\mathbf{d} \in \mathcal{L}_2$  [17]. Importantly, the result is valid irrespective of the model parameters or number of modes modelled. The simplest strictly passive feedback  $\mathbf{u} = -\mathbf{K}_d \mathbf{y}$ , where  $\mathbf{K}_d$  is diagonal with positive entries, corresponds to sensors and actuators collocated in the sense that they are at the same location and the sensor reads the components  $w_x \dot{w}_x|_{\mathbf{r}_i}$  and  $w_y \dot{w}_y|_{\mathbf{r}_i}$  with the appropriate scaling given the orientation  $\alpha_i$  of the actuator. However, control laws involving non-diagonal  $\mathbf{K}_d$  (sensor coupling) and dynamic feedbacks are also possible. This allows us to be more flexible in our design.

## 5 Simulation

The shape functions must be selected to satisfy the boundary conditions for the actual displacement  $\mathbf{u}_e$ . In both the constrained and unconstrained examples to follow, the plate is cantilevered on one side and free on the others. We select for shape functions:

$$\psi_{i=j+(k-1)n_x}(x, y) = X(x)_j Y(y)_k \quad (46)$$

Where  $X_j(x)$  is the  $j$ 'th eigenfunction (mode) of a thin free-free beam, that is, the  $j$ 'th mode of

$$\frac{\partial^4 X}{\partial x^4} - \gamma_x^4 X = 0, \quad \frac{\partial^2 X(0)}{\partial x^2} = \frac{\partial^3 X(0)}{\partial x^3} = \frac{\partial^2 X(L_x)}{\partial x^2} = \frac{\partial^3 X(L_x)}{\partial x^3} = 0 \quad (47)$$

and  $Y_k(y)$  is the  $k$ 'th eigenfunction of a thin cantilevered beam, satisfying

$$\frac{\partial^4 Y}{\partial y^4} - \gamma_y^4 Y = 0, \quad Y(0) = \frac{\partial Y(0)}{\partial y} = \frac{\partial^2 Y(L_y)}{\partial y^2} = \frac{\partial^3 Y(L_y)}{\partial y^3} = 0 \quad (48)$$

$n_x$  is the number of  $X_j(x)$  used in the approximation. To clarify the indexing, it is just the re-ordering of the matrix  $[X_1 X_2 \dots]^T [Y_1 Y_2 \dots]$  into a single vector by column concatenation. In this way all possible products of beam shape functions constitute the shape functions of the plate.



The equations of motion are written in state-space form with nonlinear output:

$$\dot{\mathbf{x}} = \mathbf{A}\mathbf{x} + \sum_{i=1}^m u_i(t)\mathbf{B}_i\mathbf{x}, \quad y_i = -\mathbf{x}^T \mathbf{\Pi}_i \mathbf{x} \quad (49)$$

where

$$\mathbf{x} = \begin{bmatrix} \mathbf{q} \\ \dot{\mathbf{q}} \end{bmatrix}, \quad \mathbf{q} = \begin{bmatrix} \mathbf{w}_0 \\ \boldsymbol{\theta} \\ \mathbf{q}_e \end{bmatrix}, \quad \mathbf{A} = \begin{bmatrix} \mathbf{0} & \mathbf{1} \\ -\mathbf{M}^{-1}\mathbf{K} & \mathbf{0} \end{bmatrix}, \quad \mathbf{B}_i = \begin{bmatrix} \mathbf{0} & \mathbf{0} \\ -\mathbf{M}^{-1}\mathbf{\Pi}_i & \mathbf{0} \end{bmatrix} \quad (50)$$

A 4<sup>th</sup>-order Runge-Kutta method is applied below to simulate the closed-loop dynamics.

### 5.1 Constrained Case

The constrained model with embedded actuators was simulated from an initial deflection of  $\eta_1(t=0) = \eta_2(t=0) = 1$ . Table 1 shows the physical parameters used.

Table 1: Physical parameters for constrained plate simulations

$N_e$	$L_x$	$L_y$	$\rho$	$\nu$	D	$f_x$	$f_y$	$\alpha$
9	5 m	10 m	1kg/m <sup>2</sup>	0.3	10Pa m <sup>3</sup>	$[0, L_x/2, L_x]$	$[L_y, 2L_y/3, L_y]$	$[9\pi/16, \pi/2, -9\pi/16]$

Here,  $f_x, f_y$  are the locations of the actuators. The side  $y = 0$  is cantilevered while the other three edges are free. In the left plot of Fig. 3, the control laws  $u_i(t) = 1000\mathbf{q}_e^T \mathbf{K}_{c,i} \dot{\mathbf{q}}_e$  N/m are used on all actuators. This is a discretized version of what might be implemented in practice with  $u_i = -1000 y_i$ . Now, suppose the output is filtered to reject noise in measurement. In addition, we notice that because the model is state-dependent, the controller has trouble reducing the small oscillations. We can use a steeper gain profile close to the origin as follows:

$$u_i(t) = - \begin{cases} S_1(r_i(t) - \epsilon) + \epsilon S_2, & r_i > \epsilon \\ S_2 r_i(t), & -\epsilon \leq r_i \leq \epsilon, \\ S_1(r_i(t) + \epsilon) - \epsilon S_2, & r_i < -\epsilon \end{cases} \quad S_2 > S_1 \geq 0, \epsilon > 0 \quad (51)$$

where  $\dot{r}_i + \lambda r_i = y_i$ ,  $\lambda > 0$ , so the controller is composed of a strictly passive linear block (the first-order filter) connected in series with a strictly passive static nonlinearity. Such a system is strictly passive [17]. This modified feedback with parameters  $(S_1, S_2) = (1000, 2E^5)$ ,  $\epsilon = 0.05\text{s}^{-1}$ ,  $\lambda = 3\text{s}^{-1}$  is used on all actuators and shown on the right in Fig. 3.

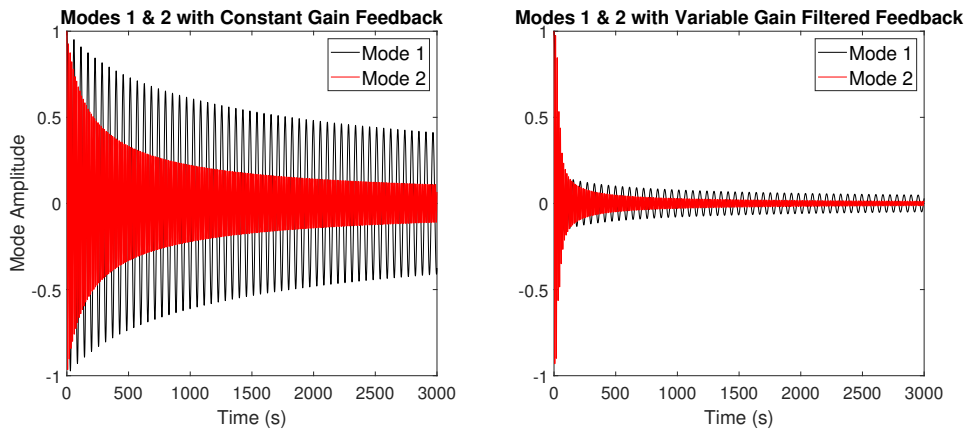


Fig. 3: Closed-loop 1<sup>st</sup> and 2<sup>nd</sup> modes with different strictly passive feedbacks for constrained model

## 5.2 Unconstrained Case

The unconstrained model with embedded actuators was simulated from an initial deflection of  $\eta_1(t=0) = \eta_2(t=0) = 1$ . Table 2 shows the physical parameters used. The  $N_e$  field means that each plate has nine elastic degrees of freedom.

Table 2: Physical parameters for unconstrained plate simulations

$N_e$	$L_x$	$L_y$	$\rho$	$\nu$	D	$f_x$	$f_y$	$\alpha$
$2 \times 9$	10 m	10 m	1kg/m <sup>2</sup>	0.3	10Pa m <sup>3</sup>	$[0, L_x]$	$[L_y, L_y]$	$[\pi/4, -\pi/4]rad$

The parameters in Table 2 apply to both plates; the spacecraft and its actuators have odd symmetry in the x-y plane. The rigid body  $\mathcal{R}$  has dimensions  $[x_{dim}, y_{dim}, z_{dim}] = [10, 10, 5]$  m and mass 500 kg. On the left in Fig. 4, we have the closed-loop response for  $u_i(t) = 5000\mathbf{q}^T \mathbf{I}_i \dot{\mathbf{q}}$ , while on the right we have the same type of variable-gain feedback as in the second constrained case with parameters  $(S_1, S_2) = (1, 5E^4)$ ,  $\epsilon = 0.0002 \text{ s}^{-1}$ ,  $\lambda = 0.25 \text{ s}^{-1}$ .

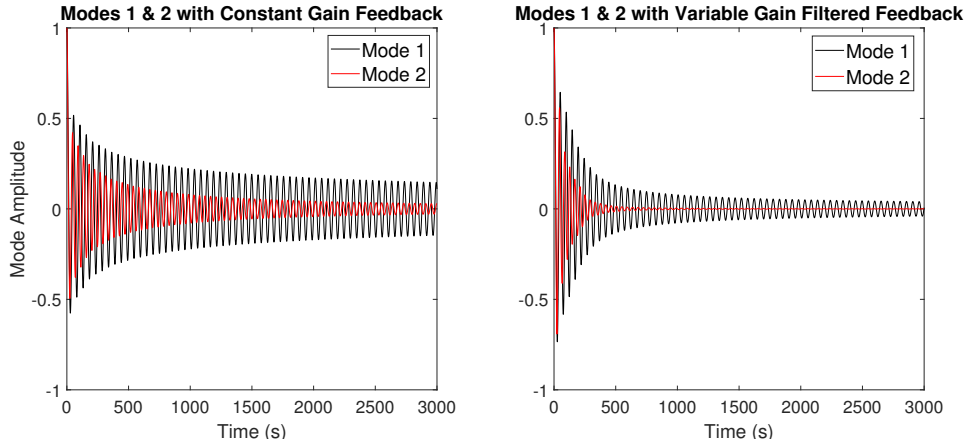


Fig. 4: Closed-loop 1<sup>st</sup> and 2<sup>nd</sup> modes with different strictly passive feedbacks for unconstrained model

## 6 Conclusion

We have investigated the effect of embedded coils of current carrying wire in flexible constrained and unconstrained structures. The resulting bilinear control problem has been approached first through an assignment to make the Lyapunov function negative. Next it was shown this technique can be generalized to strictly passive feedback controllers given that a sensor measures a generalized rate, given by x-y components of the product of slope and slope-rate. The robustness with respect to model parameter error, unmodelled passive dynamics, and finite-energy disturbances arise naturally from the passivity-based feedback technique. The main limitation to this method is that actuators/sensors must be placed away from regions where the derivatives of the natural mode shapes are zero in both directions. Simulations show some example actuator configurations that are effective at suppressing structure vibration with these feedback laws.

## References

1. D. Tzeranis and S. Dubowsky, "Vibration control in the assembly of large flexible structures by teams of space robots", *IFAC Proceedings Volume 39, Issue 15*, pp. 719-724, (2006)
2. F. Casella, A. Locatelli, N. Schiavoni, "Modeling and control for vibration suppression in a large flexible structure with jet thrusters and piezoactuators", *IEEE Transactions on Control Systems Technology Volume 10, Issue 4*, pp. 589-599, (2002)
3. T. Guo, Q. Lu, and J. Li, "PI force feedback control for large flexible structure vibration with active tendons", *Acta Mechanica Sinica, ISSN 0567-7718, Volume 24, Issue 6*, pp. 721-725 (2008)
4. C. J. Damaren and G. M. T. D'Eleuterio, "Optimal Control of Large Space Structures Using Distributed Gyricity," *AIAA J. Guidance, Control, and Dynamics*, v12, 5, pp. 723-731 (1989)
5. J.-F. Shi and C. J. Damaren, "Control law for active structural damping using a control moment gyro", *Journal of Guidance, Control, and Dynamics, ISSN 0731-509, Volume 28, Issue 3*, pp. 550 - 553 (2005)
6. Y.-R. Hu, A. Ng, "Active robust vibration control of flexible structures",
7. T. Voss, J.M.A. Scherpen, "Port-Hamiltonian modeling of a nonlinear Timoshenko beam with piezo actuation", *SIAM Journal on Control and Optimization, ISSN 0363-0129, Volume 52, Issue 1*, pp. 493-519 (2014)
8. M.A. Peck and B. Streetman, and C.M. Saa, and V. Lappas, "Spacecraft formation flying using Lorentz forces", *Journal of the British Interplanetary Society, ISSN 0007-084X, Volume 60, Issue 7*, pp. 263-267 (2007)
9. E. Silani, M. Lovera, "Magnetic spacecraft attitude control: a survey and some new results" *Control Engineering Practice Volume 13, Issue 3*, pp. 357-371 (2005)
10. M. Lovera and A. Astolfi, "Spacecraft attitude control using magnetic actuators", *Automatica, ISSN 0005-1098, Volume 40, Issue 8*, pp. 1405-1414 (2004)
11. B. Wong and C. J. Damaren, "Satellite attitude control using electrodynamic booms", *International Journal of Space Science and Engineering, ISSN 2048-8459, Volume 1, Issue 1*, pp. 51-63 (2013)
12. R. Wiśniewski, and M. Blanke, "Fully magnetic attitude control for spacecraft subject to gravity gradient", *Automatica, ISSN 0005-1098, Volume 35, Issue 7*, pp. 1201-1214 (1999)
13. G. Anastas, D. Eisenhaure, R. Hockney, B. Johnson, K. Misovec, "Distributed magnetic actuators for fine shape control", *AFAL-TR-88-026, Air Force Astronautics Laboratory, Edwards Air Force Base, California* (1988)
14. R.-F. Fung, C.-C. Wang, and Y.-T. Liu, "Dynamic model of an electromagnetic actuator for vibration control of a cantilever beam with a tip mass", *Journal of Sound and Vibration Volume 288, Issues 4-5*, pp. 957-980 (2005)
15. M. Slemrod, "Stabilization of bilinear control systems with applications to nonconservative problems in elasticity", *SIAM Journal on Control and Optimization, Volume 16, Issue 1*, pp. 131-141 (1978)
16. I. H. Shames, C. L. Dym, "Energy and finite element methods in structural mechanics", pp. 432-433, *Hemisphere Publishing Corporation*, (1985)
17. H. K. Khalil, "Nonlinear systems, third edition", pp. 227-250, *Pearson Education, Inc.* (2014)
18. C. J. Damaren, "Comments on 'Fully magnetic attitude control for spacecraft subject to gravity gradient' " *Automatica, ISSN 0005-1098, Volume 38, Issue 12*, pp. 2189-2189 (2002)
19. S. Aoues, F. L. Cardoso-Ribeiro, D. Matignon, D. Alazard, "Modeling and control of a rotating flexible spacecraft: a port-hamiltonian Approach", *IEEE Transactions on Control Systems Technology, Vol. 27, No. 1*, pp. 355-362 (2019)